Supporting Information

*Rihan Hai, Guangbin Shao, Henry Oliver T. Ware, Evan Hunter Jones, Cheng Sun,**

3D Printing a Low-cost Miniature Accommodating Optical Microscope

1. μCLIP System

This homemade μCLIP system consists of a computer for movement and projection control, a digital micromirror device (DMD) light engine (Pro 6600, Wintech Digital Systems Technology Corp.) featuring 4K resolution (3860×2160 pixels) and 385 nm UV light source, an ultraviolet (UV) projection lens (UV8040BK2, Universe Kogaku America Inc.), a resin container (installed with a piece of PDMS/Teflon membrane as oxygen permeable window) and a building stage controlled by a six-axis robotic arm (Meca500, Mecademic). As shown in **Figure S1a**, the grayscale image of each fabrication layer is loaded to the DMD light engine and the pattern is projected via UV light (λ=385 nm) into the liquid resin from below. The oxygen will diffuse through the membrane and create a so-called "deadzone" at the vicinity of the membrane, where the free radical polymerization is substantially inhibited by the oxygen. This prevents adhesion while maintaining the supply of fresh resin as the printed structure being pulled up continuously in z-direction. The light engine used in our experiment features a power density up to 30.33 mW cm^{-2}, with a projection area of 19.3×10.8 mm^2 and a high spatial resolution of 5×5 μm^2 $pixel^{-1}$.

2. Slicing and Grayscale Algorithm

The CAD models presented in this study are first processed by a slicing algorithm used in our previous work. The CAD model is first as saved in STL (Standard Triangular Language) format, as the vertex positions can be extracted from it as an array consisting of coordinates in x, y and z axis. A sequence of coordinates in z-axis, corresponding to each layer, can be determined by the layer thickness and the height of object. The cross-sections corresponding to the z-coordinates of the 3D object can be extracted and stored as binary bitmap images. For layers with changing radius (Figure S1c), the grayscale profile is determined by the interpolation of the adjacent layers (Figure S1d) to provide a smoother intensity profile between neighboring layers. The grayscale bitmaps were loaded into the light engine to serve as dynamic masks.

3. Determination of Printing Parameters

Printing parameters were determined by the speed-working curing method. The curing depth of photocurable resin can be expressed as:

$$C_d = A - D_p \times \ln(v_s) \quad (1)$$

where C_d is the curing depth, A is a constant of length unit determined by the combination of photocurable resin and the wavelength of projected data, D_p is the penetration depth of the projected UV light and v_s is the building plate moving speed. In μCLIP technique, a "deadzone" exists at the vicinity of oxygen permeable window where the photopolymerization is prohibited. The "deadzone" thickness D_z should be reduced from the theoretical curing depth in Eq. (1) to obtain the actual curing depth:

$$C_d = (A - D_z) - D_p \ln(v_s) \quad (2)$$

To determine the printing speed which creates the desired curing depth, we fixed the projected UV power density to 3.17 mW/cm^2. A ladder-shape model with beam thickness of 100 μm was printed at 10.00 μm/s, 11.11 μm/s, 12.50 μm/s, 14.29 μm/s, 16.67 μm/s and 20.00 μm/s. The printed beam thickness was measured by SEM and fitted into Eq. (2) together with printing speeds to obtain the desired printing speed.

4. Printing Process of Imaging Lens

The clear resin used for an aspherical lens consists of 97.3 wt.% HDDA (Sigma-Aldrich Inc.) as low-viscosity monomer, 2.2 wt.% Irgacure 819 (BASF Inc.) as photoinitiator and 0.5 wt.% Tinuvin 171 (BASF Inc.) as UV absorber. The chemicals were mixed and stirred by ultrasonic for 1 hour to obtain the photocurable resin. The exposure time for each 1-μm fabrication layer is 0.06 s, with an intensity of 3.63 mW cm^{-2}. The imaging lenses were printed at a linear printing speed of 16.67 μm/s. After printing, a meniscus coating process was performed for the imaging lenses to consume the residual resin and form a continuous lens profile. The residual resin was partially removed by placing delicate task wipers (Kimtech Science Kimwipes 34155, Kimberly-Clark Inc.) near the bottom of the printed lens to absorb the remaining resin. The samples were then stored in a transparent sample box, which was filled by N_2, and post cured in UV light (365 nm) for 5 min with an intensity of 74.75 mW cm^{-2}.

5. Image Tests Setup and Process for Lens

Figure S2 shows a schematic illustration of the experimental setup. A United States Air Force (USAF) 1951 resolution target was used as the test object to characterize the spatial resolutions and modulation transfer functions (MTFs) of 3D printed lenses as well as the commercial lenses. The images formed by the 3D printed lens were collected by a 10× objective lens (UPLFLN10X2, Olympus Corporation of Americas) and then projected to a complementary metal-oxide-semiconductor (CMOS) camera (EO-5012M MONO LE, Edmund Optics). Bandpass filters with different center wavelengths at 488, 532, 632.8 nm were used to provide blue, green and red illuminations, respectively. This setup was primarily used to test the standalone performance of different lenses. When testing their performances on endoscope, the "Imaging" part was substituted by the integrated endoscope; the "Object" part was replaced by biological samples without the bandpass filters.

Figure S3a demonstrates the frame captured by AM30 under broadband illumination, which shows distinctive chromatic aberration as the linewidths are larger than that of blue light illumination (λ = 488 nm, Figure S3b) and red illumination (λ = 632.8 nm, Figure S3c). Though chromatic aberration can be readily corrected under blue light illumination (Figure S3b) and red illumination (Figure S3c), the frames captured show a lower spatial resolution as the lens was optimized for green light illumination (Figure 3l). However, 3D printed lens demonstrates comparable spatial resolution and better contrast compared with commercial polymer lenses (E30 and T30) under all illumination conditions (Figure S3d to i). The imaging results further confirms the fabrication precision of 3D printed lens. The measured modulation transfer functions (MTFs) under different illuminations are depicted in Figure S3j to m, diffraction limited MTFs are also plotted as references in these figures. Measured MTFs are calculated by following equation:

$$M = \frac{I_{\max} - I_{\min}}{I_{\max} + I_{\min}} \quad (3)$$

where M is the function value, $I_{\max}$ and $I_{\min}$ are the pixel values of the brightest pixel and darkest pixel within a particular element, respectively.

The measured MTFs are extracted from Figure S3a to Figure S3i and Figure 2l to 2n for each lens under different illuminations. Each data point represents the averaged value obtained from 5

bright-dark pairs of data points extracted within each element corresponding to different spatial frequencies. The 3D printed lens shows best resolution under green illumination for most of the spatial frequencies. The 3D printed lens also shows a consistently higher performance than commercial polymer lenses in the spatial frequency range of 32 to 128 lp/mm. It is worth to note that the performance of 3D printed lens is still comparable to that of commercial polymer lenses for higher spatial frequencies even in the case of blue illumination shown in Figure S3k, where 3D printed lens has the worst overall performance along the measured spatial frequency range. Our experiments validated the performance of additive manufactured optical components against its commercial counterparts, which paves the way for the birth of the proposed 3D printed opto-mechanical system.

Figure S4 shows the imaging results of 3D printed aspherical lens following another Even Surface formula (AM43). The aspherical surface was optimized for red illumination. Figure S4a demonstrates the image acquired by 3D printed lens under red illumination (632.8 nm) and it shows the lens can distinguish the fine features of Element 5 Group 7, which corresponds to a spatial resolution of 2.46 μm, on USAF resolution target. Though the lens performance is relatively poor under blue illumination (Figure S4d), it still preserves spatial resolution comparable to commercial polymer lenses under broadband (Figure S4c) and green (Figure S4e) illuminations. The measured MTF under different illuminations shown in Figure S4b further confirms the observation about the imaging results as MTF under blue illumination is the first one to drop below the critical value of 0.2, while other MTFs show relatively higher values. The imaging results presented here further validates the flexibility of our 3D printing system and paves the way to the fabrication of highly customized optical components.

6. Printing Process of Optomechanical Components

The opaque resin used for the mechanical elastic lens holder, and the lower and upper shells consist of 97.3 wt.% HDDA (Sigma Aldrich Inc.), 2.2 wt.% Irgacure 819 (BASF Inc.) and 0.5 wt.% Sudan Black I as dye. The chemicals were mixed and stirred by ultrasonic for 1 hour to obtain the photocurable resin. All the optomechanical components are loaded onto the printing bed simultaneously and printed in a single batch (Figure S1b) to reduce the fabrication time. They were fabricated with a 5-μm layer thickness and an exposure time per layer of 0.6 s, with

an intensity of 8.60 mW cm^{-2}. After printing, the printed parts were rinsed in ethanol to wash off the residual resin and were dried with air.

7. Assembly Process of Miniature Microscope

Sub-components of the microscope are assembled and then integrated into the final assembly. Front cap, lens assembly and clamshells are assembled as subsystems shown in Figure 1d. Mating features (green arrows) on each component assist alignment during assembling. UV epoxy (NOA81, Norland Products) was applied (areas designated with red dots in Figure 1b) and cured with UV illumination (365 nm, 56 mW cm^{-2}) for 20 seconds to ensure secure attachment. No additional alignment processes or equipment is needed for the installation. The VCM was assembled by first inserting the coil between the contact structures on the clamshells and fixed by UV epoxy applied at the highlighted areas (red dots). The assembled elastic lens mount was then inserted into the coil tube. The embedded grooves on the front cap will fix its alignment and rotation with respect to the clamshells. The gap between two hemi-circular skirts will fix the position of the elastic lens mount by trapping the contact features on the side walls of the lens holder. Finally, UV epoxy was applied at highlighted areas on the outer body of the microscope to finalize the assembly and the experimentally assembled microscope is shown in Figure 1e. The video showing the whole assembly process can be found in the **Supplementary Movie S1**.

8. Imaging Tests and Image Processing for Assembled Microscope

Imaging tests with biological specimens were performed using miniature microscopes assembled with AM30, E30 and T30 for comparison and focus stacking. The experimental setup is the same as shown in **Figure S2**. However, the filter was removed to provide broadband illumination and the "Imaging" section was replaced by the assembled microscope. The assembled microscope was fixed on the objective bases on a microscope (Olympus IX81). Three different combinations of biological samples were used as imaging objects: housefly labellum/honeybee barsitarsus (Case I), housebee glossae/honeybee barsitarsus (Case II) and two pieces of onion epidermis (Case III). In each case, the two samples were separated 1.0 mm vertically and 0.8-1.2 mm horizontally. The miniature microscope was first brought into focus on one of the samples by tuning the knob of the microscope. Then we turn on the power supply connected to the coil to provide magnetic force and use the VCM to scan the lens axially. A scan cycle records the focusing on object A, focus changing from object A to object B and focusing back on object A.

Real time captured videos consist of several scan cycles for three lenses imaging different cases are found in the **Supplementary Movie S2-S4** (AM30), S5-S7 (E30), and S8-S10 (T30), respectively. Frames for focus stacking are randomly chosen from a single scan cycle and are used for focus stacking after color correction described in **Figure S5**. A background image (Figure S5a) without any object was taken using the experimental setup described above. In Figure S5a, the vignetting on CMOS sensors is clearly shown on the corners and borders of the figure. The average RGB values are calculated from the central region (red dotted box in Figure S5a) and used as standard RGB values. Element-wise difference between the standard RGB values and RGB values on each pixel of the background image are calculated and resulted in the color mask shown in Figure S5b. For each original image extracted from the videos, the color mask was subtracted from them as shown in Figure S5c. The aforementioned color shift can also be observed from the image shown in Figure S5c. After color correction, Figure S5d shows the color corrected image in which no significant color shift is observed.

Figure S6 demonstrates the focus stacking results acquired by E30 installed on 3D printed microscope. The lens can distinguish the network structure on the house fly labellum (Figure S6a) but cannot resolve the fine hairs on the honeybee barsitarsus (Figure S6b). Overall, the miniature microscope equipped with E30 can achieve the desired focus stacking feature for Case I samples (Figure S6c) but with much reduced details compared with images acquired by AM30 (Figure 4c). Furthermore, E30 fails to image the fine segments on housebee glossae (Figure S6d, Case II). Combined with its poor performance on imaging the fine hairs on honeybee barsitarsus, this leads to failure of reconstructing meaningful focus stacking results for Case II. Finally, E30 shows a reduced contrast of the cell walls in onion epidermis samples (Figure S6g, h) compared with AM30 (Figure 4g and 4h) and the cell walls shown in Figure S6i are substantially less distinctive than those in Figure 4i. The defects in single frames lead to the overall low quality and failure in focus stacking shown Figure S6c, f and i.

Figure S7 presents the focus stacking results acquired by T30 installed on 3D printed microscope. The lens can distinguish the network structure on the house fly labellum (**Figure S7a**) but show lower resolution for the fine hairs on the honeybee barsitarsus (Figure S7b). The focus stacked image of Case I from T30 (Figure S7c) shows a higher contrast than that from E30, but still has lower contrast and less details compared with image acquired by AM30 (Figure 4c).

T30 also fails to image the fine segments on housebee glossae (Figure S7d). The features of housebee glossae are completely lost in the final focus stacked image (Figure S7f). Finally, for Case III, the single frames captured by T30 (Figure S7g, h) show lower contrast than the images acquired by AM30 (Figure 4g and 4h). This directly leads to the failure of focus stacking shown in Figure S7i, which has a large mistakenly reconstructed area.

9. Manufacturing Cost estimation of 3D Printed Microscope

9.1 Cost estimation of consumable materials

The oxygen permeable membrane and resin will both be consumable in the 3D printing process. The resins for imaging lens and optomechanics follow different recipes introduced in sections **4. Printing Process of Imaging Lens** and **6. Printing Process of Optomechanical Components**. Their unit prices are 0.339 $/g and 0.34 $/g, respectively. Detailed cost breakdowns are summarized in Table S1 and Table S2. All the 3D printed components are weighed using Excellence XSR Analytical Balance (Mettler Toledo). All the optomechanical components have the total weight of 0.649 g, which corresponds to the resin cost of $0.22. The 3D printed aspherical lens has the weight of 0.024 g, which corresponds to the total resin cost of $0.008.

Both AF2400 Teflon (Biogeneral Inc.) and homemade PDMS membranes are used in this study as the oxygen permeable membrane. The cost for the Teflon membrane is $800/ft for a stripe 3.5 in width, which corresponds to the unit cost of $19 per in^2. It is true that the Teflon membrane can be expensive for large area 3D printers, but for our printer with printing area of 1 in. in diameter, the cost to us is marginal. We have carefully designed the resin bath to effectively clamp down and tension the Teflon membrane to maximize its utilization. The Teflon membrane is mechanically strong, and in our daily operation, can last for 3 months or longer. This corresponds to a running cost of $19 / 90 days / 24 hours = $ 0.009.

For the home-made PDMS membrane, the price of a 500g PDMS curing kit (Sylgard 184 Elastomer Curing Kit, Dow Inc.) is $286.15, which corresponds to a unit price of $0.57 per gram. To make the estimation safer, let’s assume a 10% residual ratio (which is highly overestimated), leading to an updated unit price of $0.64 per gram. Each piece of PDMS film used in our case weighs around 0.06g and each of them can produce ~60 lenses before being

replaced. The cost added to our system from using PDMS membrane for optical components is (0.64 $/g × 0.1 g)/60, coming out to $0.0006.

9.2 Cost estimation of the capital equipment

A summary of the cost breakdown of the home-made μCLIP systems used in this study can be found in Table S3.

The total capital cost is $23,930. It is worthwhile to note that the 6-Dof robot arm is an unnecessarily complex component for this project, but that it happened to be the system available for this study. For the interest of cost reduction, it can be replaced with a linear motorized stage (X-LRT0100AL-AE53C-KX14N, Zaber Inc.) for the cost of $4,534, reducing capital cost down to $14,457. Nevertheless, we will still use the cost of the current system in the following estimation.

Using a moderate estimation, this cost is depreciated over a 10-year period and considered a zero residual value (which incidentally overestimates the cost), resulting in the annual equipment cost of $2,396. The corresponding hourly cost is $2,396/(260 workdays)/(8 hours per workday), which is roughly $1.15. Since the total fabrication time is 45 min. 21s, then the depreciation cost added to each microscope is $0.87. The cost estimate shown in Table 1 in the manuscript include the cost for consumable materials and the capital equipment appreciation. However, the cost of the man-power is not included in the calculation.

Chemicals	Ratio (wt. %)	Unit Price ($/g)
HDDA (1,6-Hexanediol Diacrylate)	97.3	0.206
Irgacure 819	2.2	5.62
Sudan Black I	0.5	3.236
	Total Cost:	0.340

Table S1. Cost breakdown of the resin used for fabricating optomechanical components.

Chemicals	Ratio (wt. %)	Unit Price ($/g)
HDDA (1,6-Hexanediol Diacrylate)	97.3	0.206
Irgacure 819	2.2	5.62
Tinuvin 171	0.5	2.992
	Total Cost:	0.339

Table S2. Cost breakdown of the resin used for fabricating optical lenses.

Components	Model, Manufacturer	Cost
UV Light Engine	Pro 6600, Wintech Digital Systems Technology Corp. 3860×2160 pixels	$6,473
UV projection lens	UV8040BK2, Universe Kogaku America Inc.	$1,350
6-DoF Robot Arm	Meca500, Mecademic Inc.	$14,040
Resin Bath	Custom CNC	$100
Optomechanical Components	Thorlabs Inc.	$1,000
Computer	Dell	$1,000
	Total Cost:	$23,963

Table S3. Cost breakdown of the μCLIP 3D printer used in this study.

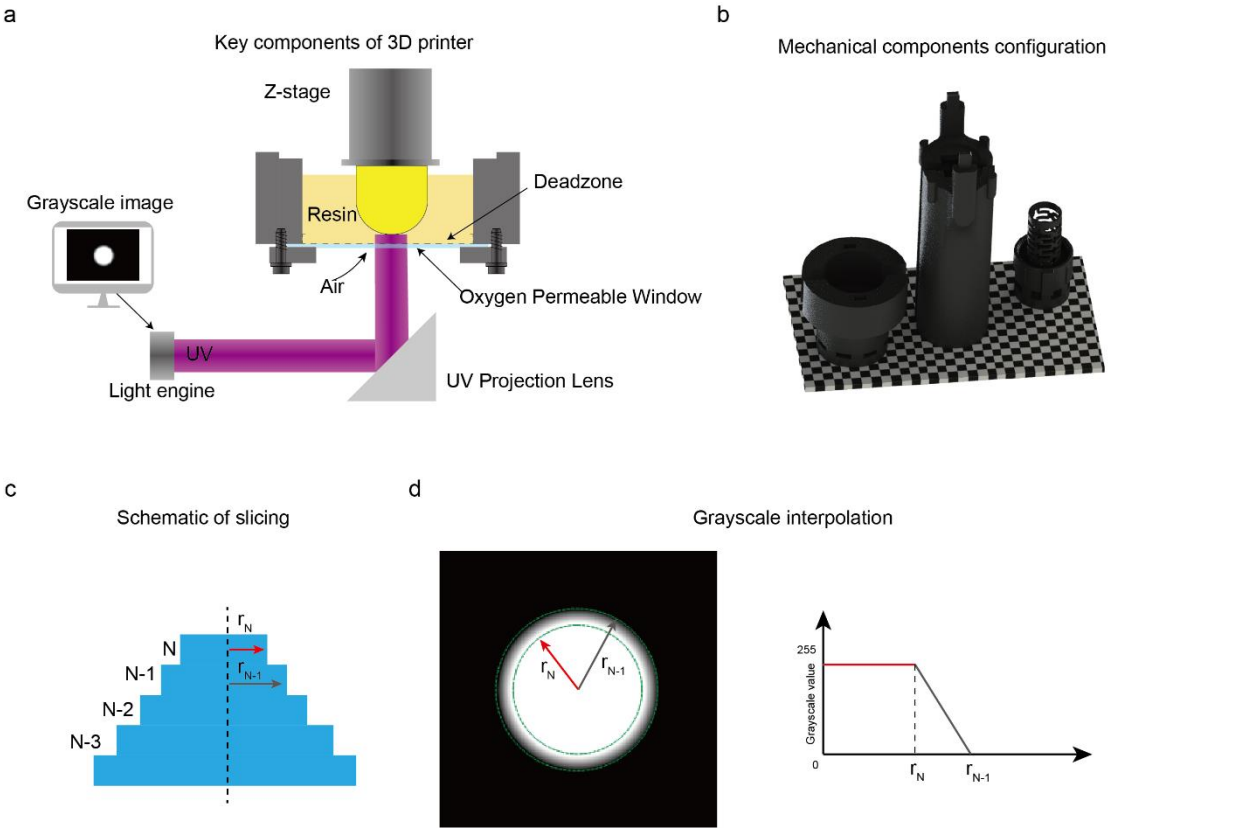

Figure S1. a) Schematic of key functional components of micro-Continuous Liquid Interface Production (μCLIP) 3D printing system. b) Configuration of mechanical components on the printing bed for the unified printing. c) Schematic of slicing layers. d) Schematic illustration of grayscale interpolation.

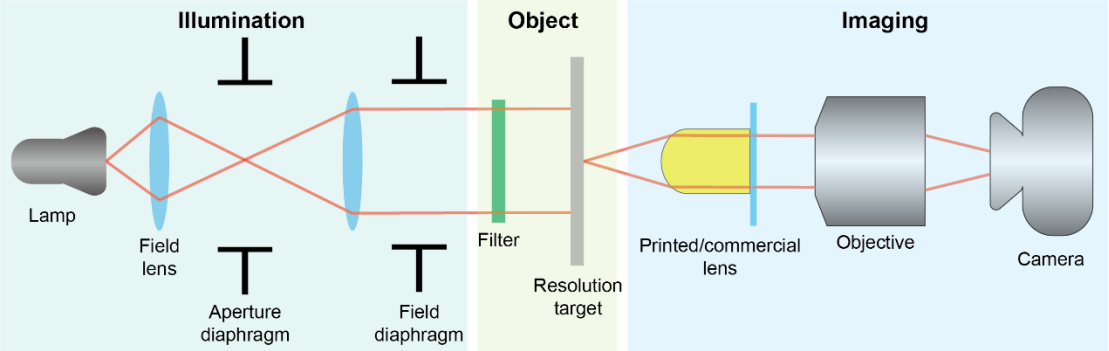

Figure S2. Schematic of optical test system to characterize the imaging quality of printed lens.

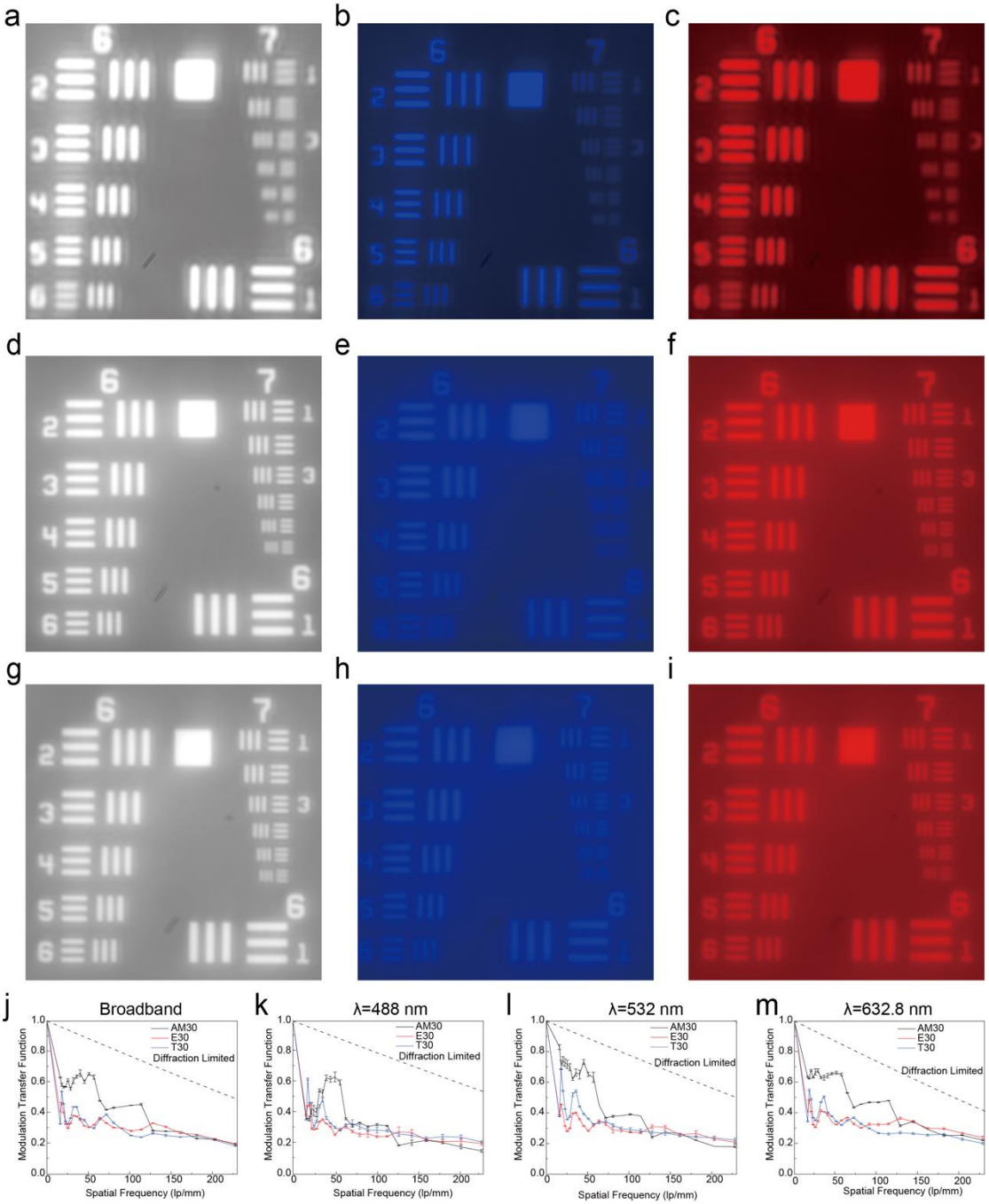

Figure S3. a-c) Images acquired by 3D printed aspherical lens from USAF 1951 resolution target under broadband, 488 nm (blue) and 632.8 nm (red) illuminations, respectively. d-e) Images acquired from the same target by molded acrylic aspherical lens from Thorlabs, Inc. (APL0303, Thorlabs, Inc.) under broadband, 488 nm and 632.8 nm illuminations, respectively. g-i) Images acquired from the same target by plastic aspherical lens (15-271, Edmund Optics). j-m) Measured modulation transfer functions (MTFs) of 3D printed lens and two commercial polymer lenses under j) broadband illumination, k) 488 nm (blue light) illumination, l) 532 nm (green light) illumination and m) 632.8 nm (red light) illumination. The black dotted lines are diffraction limited MTFs under corresponding illuminations.

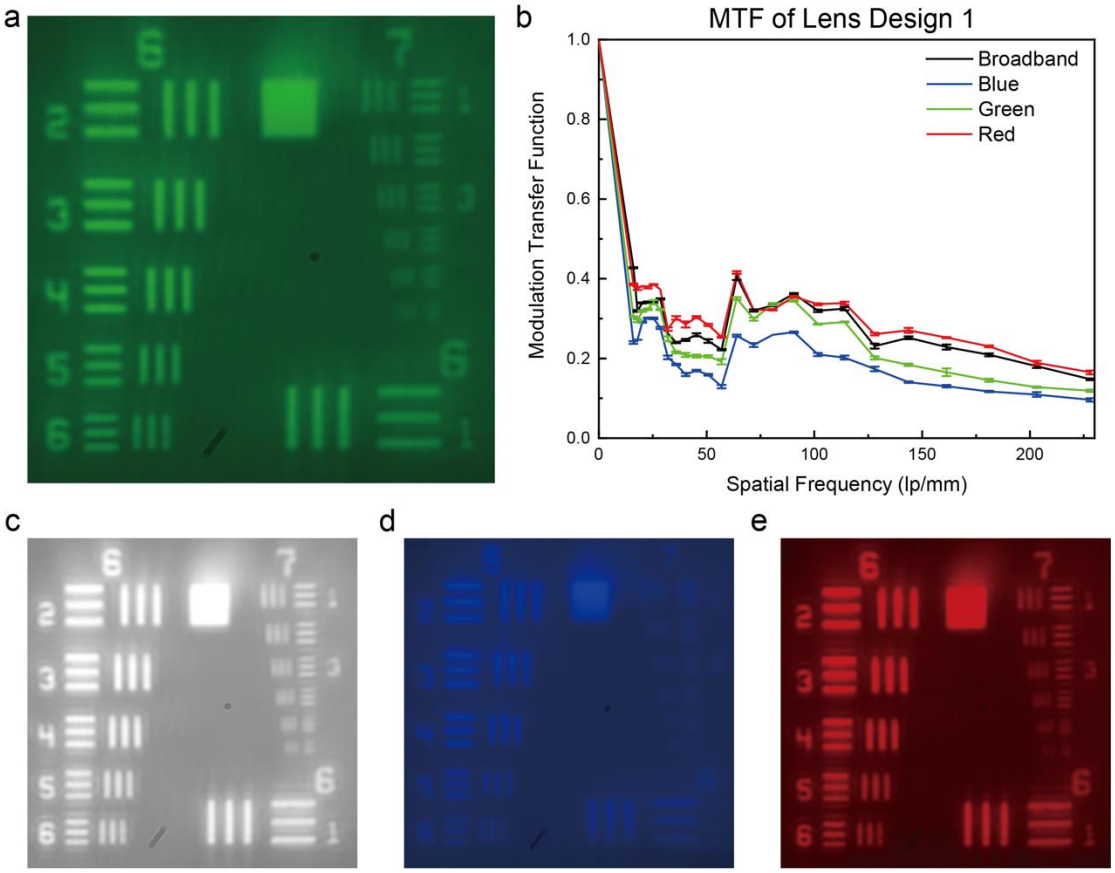

Figure S4. Images acquired by AM43 under a) green illumination (532 nm), c) broadband illumination, d) blue illumination (488 nm) and e) red illumination (632.8 nm) and b) extracted MTF.

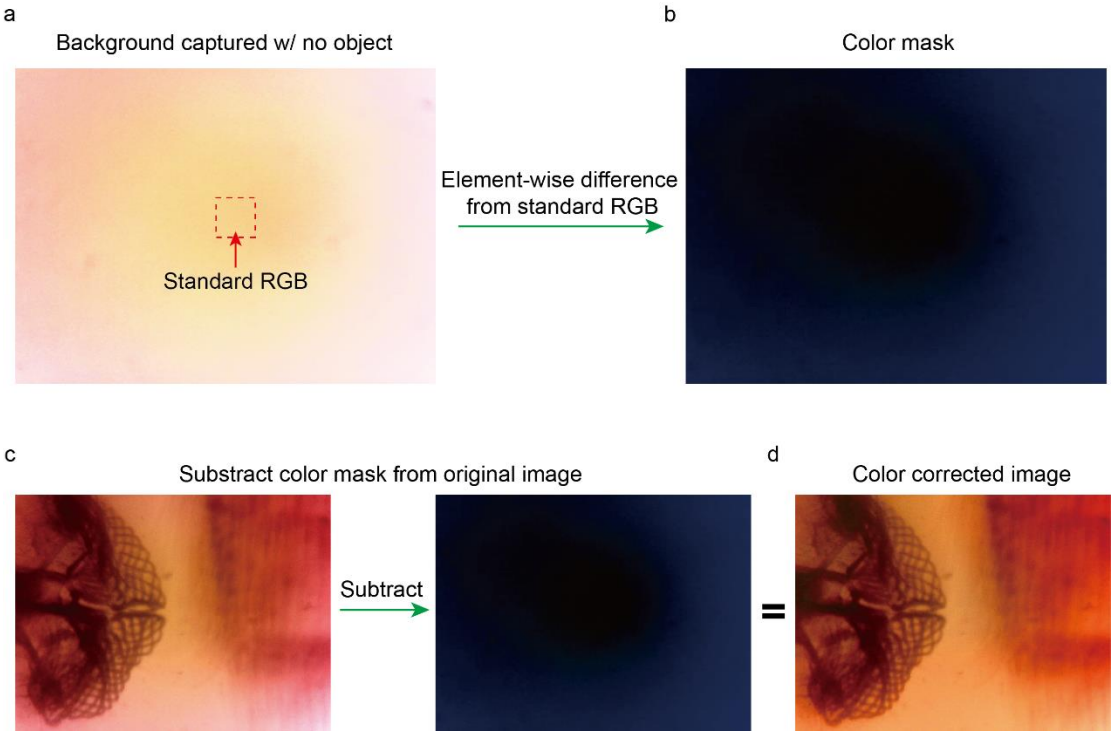

Figure S5. Color correction algorithm applied to single frames. a) Color background used to calculate the color mask for color correction. b) Color mask obtained by calculating the element-wise difference between the standard RGB value. c) The color mask is subtracted from the original image. d) Color corrected image used for focus stacking.

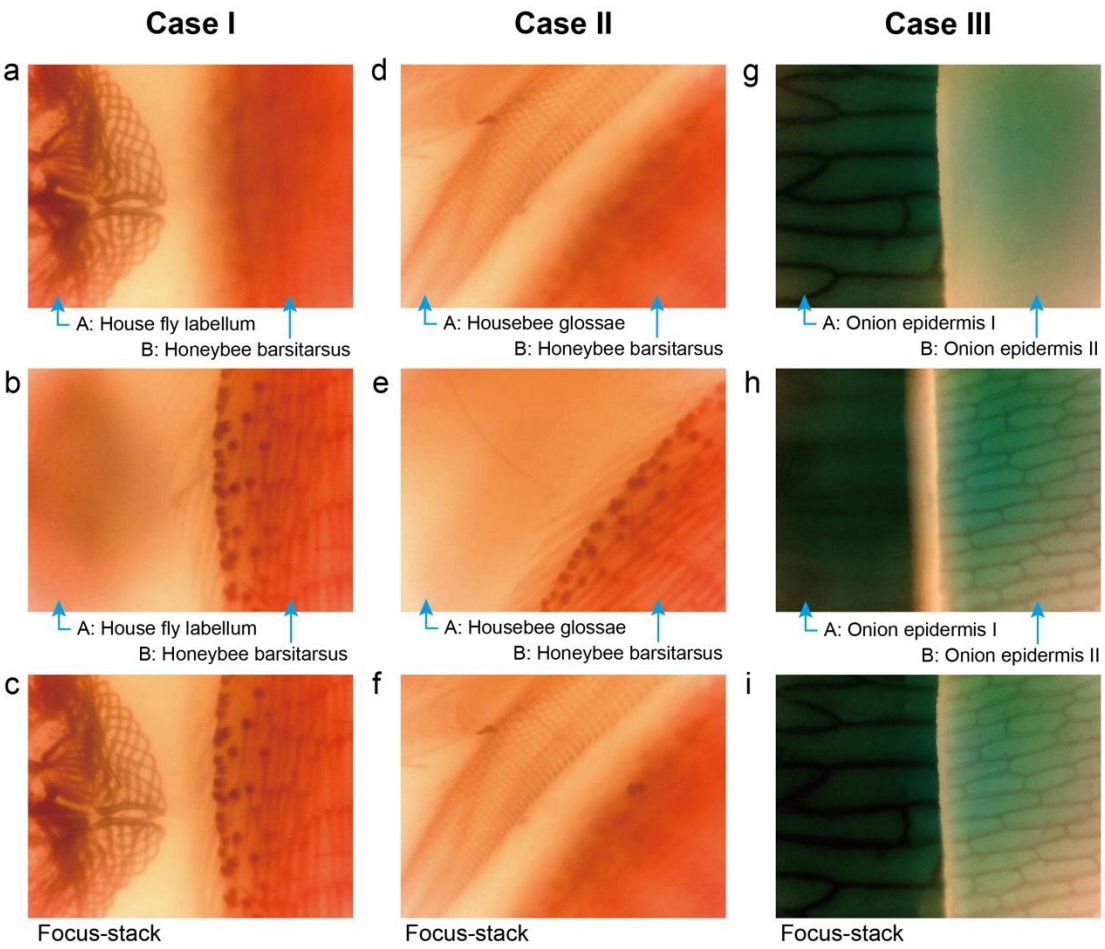

Figure S6. Focus stacking results of 3D printed microscope installed with E30. Case I: a) focusing on house fly labellum, b) focusing on honeybee barsitarsus and c) focus stacked images. Case II: d) focusing on housebee glossae, e) focusing on honeybee barsitarsus and f) focus stacked images. Case III: g) focusing on epidermis I, h) focusing on epidermis II and i) focus stacked images.

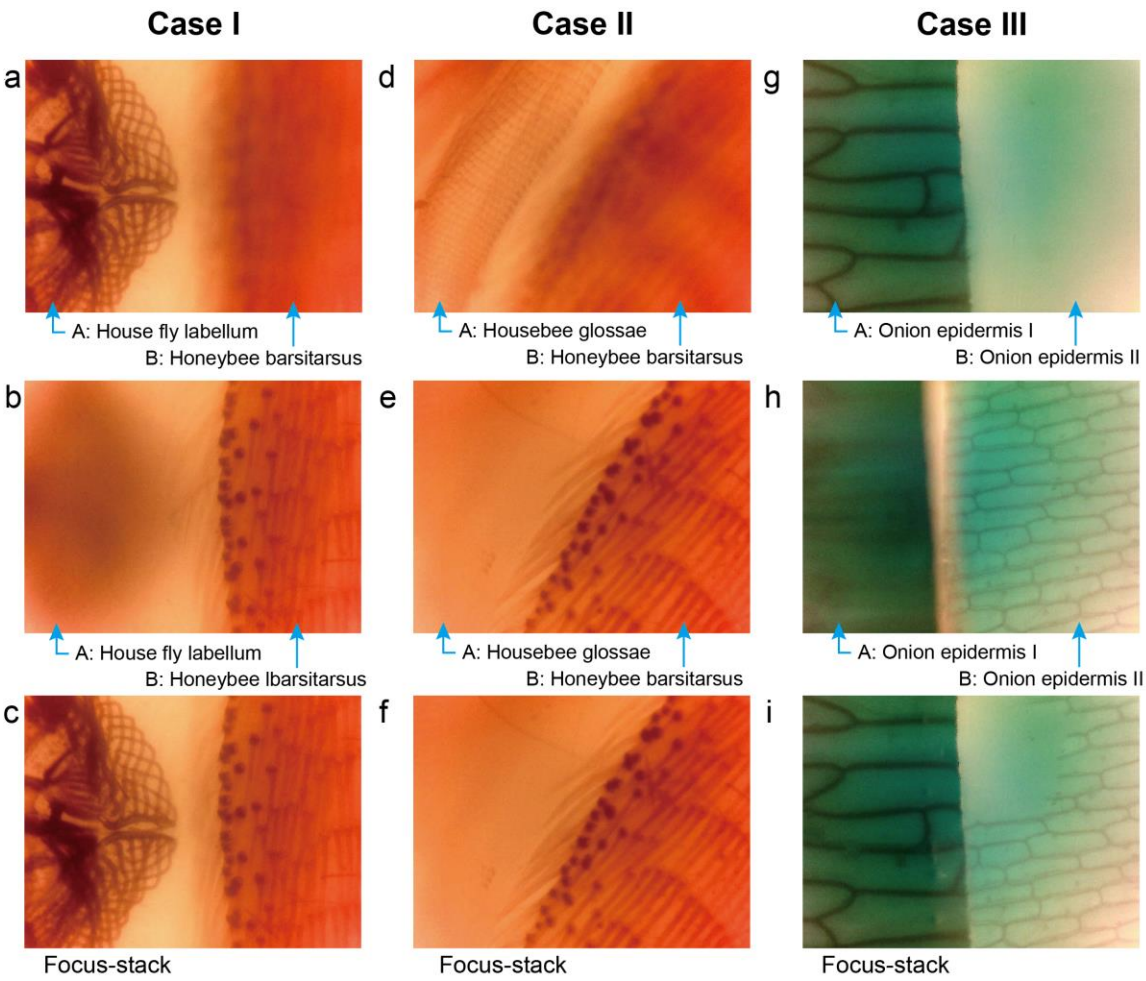

Figure S7. Focus stacking results of 3D printed microscope installed with T30. Case I: a) focusing on house fly labellum, b) focusing on honeybee barsitarsus and c) focus stacked images. Case II: d) focusing on housebee glossae, e) focusing on honeybee barsitarsus and f) focus stacked images. Case III: g) focusing on epidermis I, h) focusing on epidermis II and i) focus stacked images.

Captions for Supplementary movies

Supplementary movie S1. The video showing the process of assembling the miniaturized accommodating optical microscope using 3D printed and off-the-shelf components.

Supplementary movie S2. Recorded video for imaging pair of house fly labellum (object A) and honeybee barsitarsus (object B) specimens (Case I) while axially translating 3D printed Lens (AM30) using the build-in VCM.

Supplementary movie S3. Recorded video for imaging pair of labial palp (object A) and honeybee barsitarsus (object B) specimens (Case II) while axially translating 3D printed Lens (AM30) using the build-in VCM.

Supplementary movie S4. Recorded video for imaging two pieces of onion epidermis (Case III) while axially translating 3D printed Lens (T30) using the build-in VCM.

Supplementary movie S5. Recorded video for imaging pair of house fly labellum (object A) and honeybee barsitarsus (object B) specimens (Case I) while axially translating polymer lens from Thorlabs (T30) using the build-in VCM.

Supplementary movie S6. Recorded video for imaging pair of labial palp (object A) and honeybee barsitarsus (object B) specimens (Case II) while axially translating polymer lens from Thorlabs (T30) using the build-in VCM.

Supplementary movie S7. Recorded video for imaging two pieces of onion epidermis (Case III) while axially translating polymer lens from Thorlabs (T30) using the build-in VCM.

Supplementary movie S8. Recorded video for imaging pair of house fly labellum (object A) and honeybee barsitarsus (object B) specimens (Case I) while axially translating polymer lens from Edmund Optics (E30) using the build-in VCM.

Supplementary movie S9. Recorded video for imaging pair of labial palp (object A) and honeybee barsitarsus (object B) specimens (Case II) while axially translating polymer lens from Edmund Optics (E30) using the build-in VCM.

Supplementary movie S10. Recorded video for imaging two pieces of onion epidermis (Case III) while axially translating polymer lens from Edmund Optics (E30) using the build-in VCM.